

Tuning the Transport Properties of Gases in Porous Graphene Membranes with Controlled Pore Size and Thickness

Timur Ashirov, A. Ozgur Yazaydin, and Ali Coskun*

Porous graphene membranes have emerged as promising alternatives for gas-separation applications due to their atomic thickness enabling ultrahigh permeance, but they suffer from low gas selectivity. Whereas decreasing the pore size below 3 nm is expected to increase the gas selectivity due to molecular sieving, it is rather challenging to generate a large number of uniform small pores on the graphene surface. Here, a pore-narrowing approach via gold deposition onto porous graphene surface is introduced to tune the pore size and thickness of the membrane to achieve a large number of small pores. Through the systematic approach, the ideal combination is determined as pore size below 3 nm, obtained at the thickness of 100 nm, to attain high selectivity and high permeance. The resulting membrane shows a H₂/CO₂ separation factor of 31.3 at H₂ permeance of 2.23 × 10⁵ GPU (1 GPU = 3.35 × 10⁻¹⁰ mol s⁻¹ m⁻² Pa⁻¹), which is the highest value reported to date in the 10⁵ GPU permeance range. This result is explained by comparing the predicted binding energies of gas molecules with the Au surface, -5.3 versus -21 kJ mol⁻¹ for H₂ and CO₂, respectively, increased surface-gas interactions and molecular-sieving effect with decreasing pore size.

is a trade-off between these two metrics, resulting in membranes with either high permeance or high selectivity but not both.^[5-7] The ideal membranes, however, should have both high permeance and high selectivity, enabling a significantly lower membrane footprint.

2D materials such as graphene^[8-16] and transition metal dichalcogenides^[16-21] have gained tremendous importance as membrane materials due to their mechanical stability and atomic thickness. The impermeability of graphene, however, requires advanced pore engineering techniques.^[22] These techniques involve ultraviolet (UV)-induced and/or oxygen plasma etching and focused ion beam (FIB) irradiation with/without subsequent chemical etching.^[23] The plasma etching techniques are hard to control and lead to either very low porosity or non-uniform pores. This is due to the fact that increasing the plasma etching time induces pore


widening rather than the formation of new pores.^[23] On the other hand, FIB irradiation can create a large number of uniformly sized pores, however, achieving pore sizes below 5 nm is challenging.^[24] Celebi et al. demonstrated a systematic approach for manufacturing porous graphene (PG) using FIB irradiation and showed gas flow kinetics across the pore sizes ranging from 76 nm to 1 μm. The graphene membrane with 76 nm pores showed incredible permeance of ≈2 × 10⁸ GPU (1 GPU = 3.35 × 10⁻¹⁰ mol s⁻¹ m⁻² Pa⁻¹) with a H₂/CO₂ separation factor of 3.67 due to the Knudsen diffusion.^[8] Knudsen diffusion is the mechanism where the separation occurs due to differences in the mass of the components and is limited to the square root of the masses ratio according to Graham's law.^[25] Boutilier et al. used an ion bombardment technique followed by O₂ plasma to create pores on graphene and showed the possibility of exceeding Knudsen selectivity. They achieved a H₂/CO₂ selectivity of ≈7, however, H₂ permeance was only ≈3000 GPU.^[26] In another study, Lee et al. applied ozone plasma to etch the pores on graphene and achieved H₂/CO₂ selectivity of 6.9 and H₂ permeance of 328 GPU.^[14] As is evident from these studies, though plasma-etching techniques enhance the selectivity by facilitating a molecular-sieving effect, they result in low permeance due to the low porosity of membranes. Another approach is to coat the PG surface with functional materials in order to form a selective layer. He et al. used polymers of intrinsic microporosity-1 (PIM-1) as the selective layer on the PG and achieved a H₂/N₂ selectivity of 20.8 at

1. Introduction

Membranes play a major role in the separation industry, mainly due to their high energy efficiency, low operational costs, durability, and continuous separation.^[1,2] Gas-separation membranes offer numerous advantages over conventional techniques such as pressure-swing adsorption^[3] and cryogenic distillation.^[4] Permeance and separation factors are the critical metrics governing the membrane performance. There

T. Ashirov, A. Coskun
Department of Chemistry
University of Fribourg
Fribourg 1700, Switzerland
E-mail: ali.coskun@unifr.ch

A. O. Yazaydin
Department of Chemical Engineering
University College London
Torrington Place, London WC1E 7JE, UK

 The ORCID identification number(s) for the author(s) of this article can be found under <https://doi.org/10.1002/adma.202106785>.

© 2021 The Authors. Advanced Materials published by Wiley-VCH GmbH. This is an open access article under the terms of the Creative Commons Attribution-NonCommercial-NoDerivs License, which permits use and distribution in any medium, provided the original work is properly cited, the use is non-commercial and no modifications or adaptations are made.

DOI: 10.1002/adma.202106785

H₂ permeance of 3130 GPU.^[27] Whereas thick polymer coating as the selective layer decreases the permeance owing to the lack of direct pores, thin layers suffer from defects and cracks leading to losses in gas selectivity.^[28] Recently, we have demonstrated the concept of adsorptive separation in the graphene-based membranes through the deposition of metal micro islands such as Pd and Ni onto PG membrane to control the transport properties of a single gas in binary gas mixtures—namely, H₂ in H₂/He and CO₂ in H₂/CO₂, respectively—thus enabling ultrahigh permeance and exceptional selectivity.^[29] Pd-coated membranes, however, require a thermal regeneration step owing to the saturation of surface binding sites. These results demonstrate that achieving high permeance and high selectivity simultaneously on graphene membranes requires an additional selective layer^[29] and/or large number of small pores (<3 nm). In this direction, herein, we demonstrated that gold (Au) deposition onto PG enables a controlled pore-narrowing strategy to achieve a large number of pores below 3 nm. By systematically increasing the membrane thickness upon step-wise deposition of Au layer, we observed a clear trend in the separation mechanism by transitioning from Knudsen diffusion to surface diffusion and eventually to molecular sieving (Figure 1) along with increased gas–surface interactions in agreement with the decreased pore size. We identified the ideal pore size of below 3 nm at the membrane thickness of 100 nm to achieve a H₂/CO₂ separation factor of 31.3 at H₂ permeance of 2.23 × 10⁵ GPU, which is the highest value reported to date in the ultrahigh permeance range.

2. Results and Discussion

Graphene was transferred onto a holey silicon nitride (SiN_x) support with 20 × 20 array of pores in the range of 500–1000 nm using a previously reported facile photoresist-based method (Figure 1A),^[29] which enables a crack-free

graphene transfer (Figure S1A,B, Supporting Information). In a typical membrane, there are 26 of such arrays on a single 15 × 15 mm sized membrane chip with a membrane area of approximately 225 mm². To ensure full coverage of the SiN_x holes and to avoid the formation of tears and cracks, we employed a double-layer graphene. PG membranes were prepared by FIB milling technique to achieve uniformly sized pores with high porosity (Figure 1B). Additionally, the FIB milling is controllable and provides good reproducibility and repeatability compared to other pore creation methods.^[24] We fabricated a large number of pores (Figure 2A) with an average size of 30.1 nm by using 30 kV voltage and 10 pA of current (Figure S1C,D, Supporting Information). The pore size histogram of the fabricated pores shown in the scanning electron microscopy (SEM) images in Figure 2A has a Gaussian-shaped pore size distribution which is typical for the pores fabricated using FIB milling (Figure 2B).^[24] Pores on the graphene surface were characterized using transmission electron microscopy (TEM) images, revealing a large number of pores ranging from 30 to 40 nm (Figure 2C). Step-wise deposition of Au layer was performed and the membrane was characterized after each step. In order to demonstrate the reproducibility and repeatability aspect of the proposed approach, three identical membranes (M1, M2, and M3) were prepared with similar pore sizes and porosities.

As expected, porous double-layer graphene (PDG) membrane exhibits a flow that can be described by the Knudsen diffusion mechanism (Figure 1C),^[8] with H₂ having the highest permeance among other gases (Figure 3A). The average permeance (*P*) versus molecular weight (*m*) curve of the PDG fits the power relation^[8] of

$$P = 3.29 \times 10^7 \times m^{-0.41} \quad (1)$$

In addition, the respective H₂/He, H₂/CH₄, H₂/N₂, and H₂/CO₂ selectivity values of the PDG membranes were found to be below respective Knudsen selectivity values (Figure 3). After the

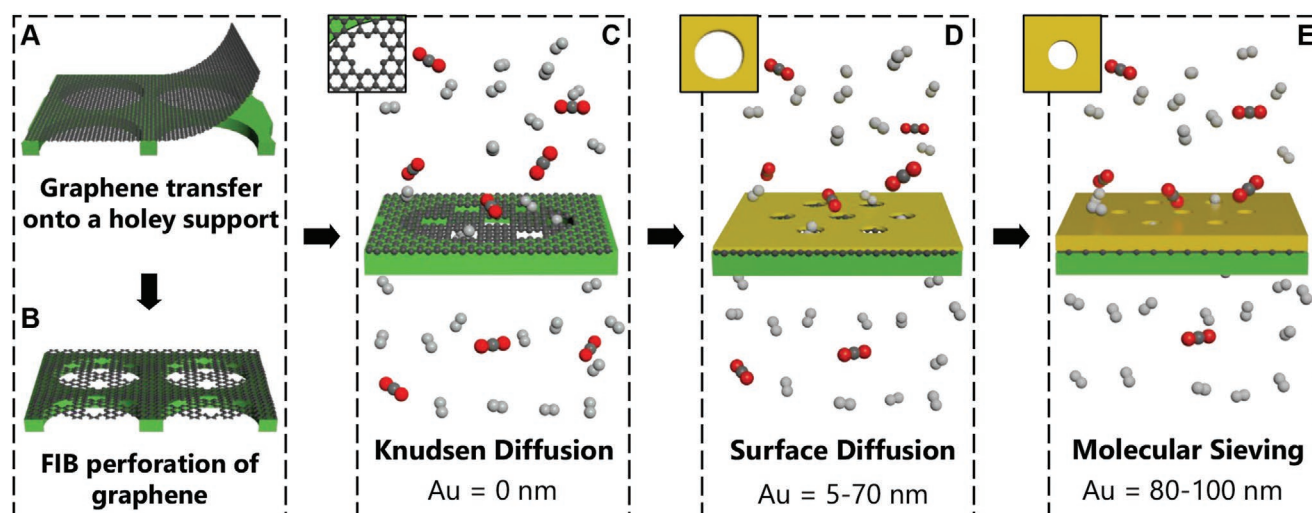


Figure 1. Schematic representation of the membrane fabrication process and separation mechanisms. A) Graphene transfer onto a holey SiN_x support using a facile photoresist-based method. B) Perforation of the graphene using FIB milling. C) Gas separation in a pristine PG membrane follows Knudsen diffusion. D) Upon deposition of a Au layer, the mechanism starts to follow the surface diffusion mechanism by faster H₂ permeation. E) Further deposition of Au layer alters the separation mechanism by transforming it into molecular sieving.

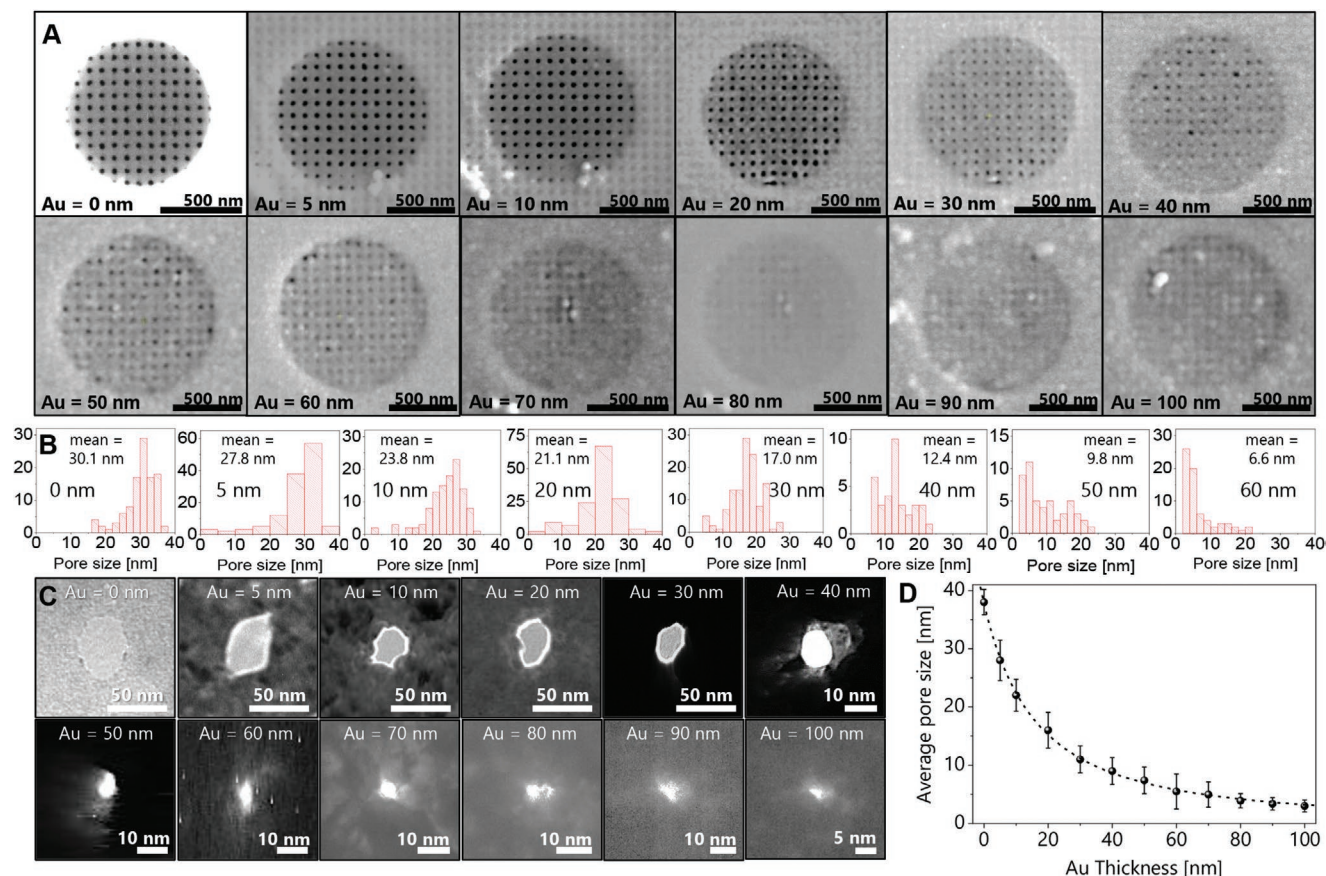


Figure 2. A) SEM images of the single ≈ 850 nm SiN_x hole coated with perforated graphene and being coated with subsequent Au depositions. The average pore size decreases upon Au deposition, eventually almost being blocked. B) Pore size distribution histograms of the samples represented in (A). The number in the middle represents the Au layer thickness C) Bright-field TEM images of the graphene holes subsequently coated by gold deposition. D) Average pore size versus thickness of the deposited Au layer.

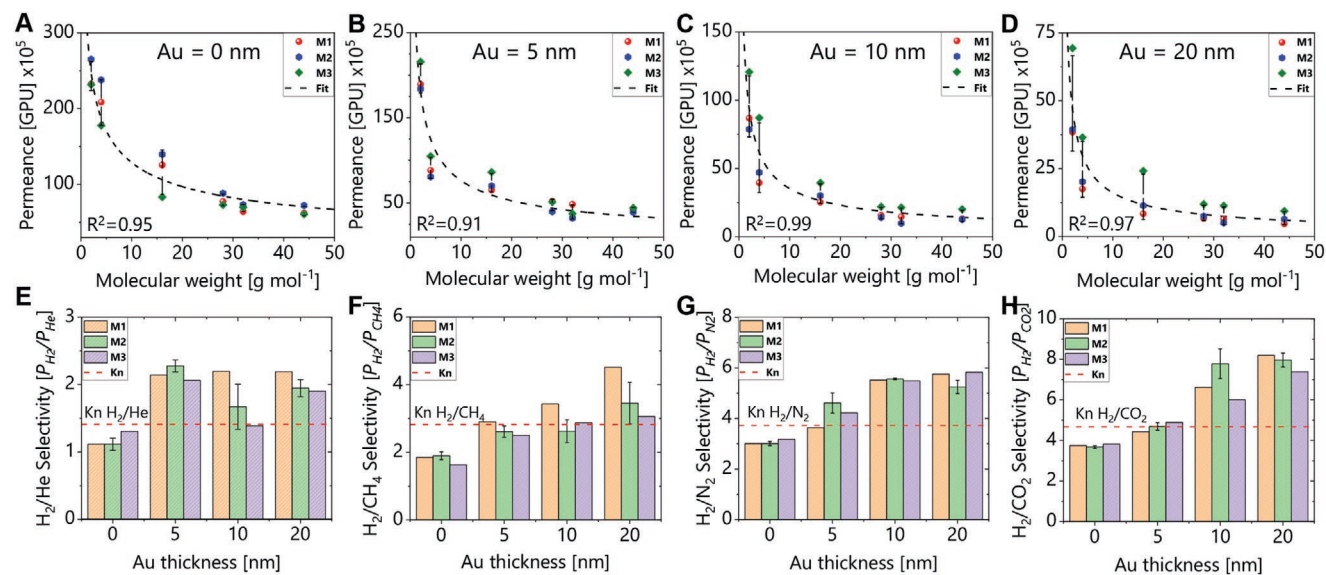


Figure 3. A) GPU versus molecular weight of the gases for pristine double-layer graphene membranes. B–D) After deposition of 5 nm (B), 10 nm (C), and 20 nm (D) of Au layer. E–H) Graphs of H_2/He (E), H_2/CH_4 (F), H_2/N_2 (G), and H_2/CO_2 (H) selectivity versus Au layer thickness for the membranes M1, M2, and M3. The red dashed line indicates the Knudsen selectivity value for the respective gas pairs.

deposition of a 5 nm Au layer, the average pore size was reduced to 27.8 nm (Figure 2A,B). The reduction in the pore size can be clearly observed from the TEM images in Figure 2C. Similarly, the permeance of the gases decreased slightly, however, the permeance versus molecular weight curve deviated from the Knudsen diffusion by favoring H₂ (Figures 1D and 3B). The power relation between permeance and molecular weight became steeper by fitting the

$$P = 2.62 \times 10^7 \times m^{-0.54} \quad (2)$$

This leads to an increase in the H₂/gas selectivity values. The H₂/He selectivity surpasses the Knudsen value at 5 nm of Au deposition while the H₂/CH₄, H₂/N₂, and H₂/CO₂ selectivity values reach the Knudsen selectivity values (Figure 3). However, the H₂/gas selectivity of the PDG was not expected to increase as the pore size is still too large for molecular sieving to occur. This increasing trend can only be explained by the faster H₂ permeation compared to other gases on the Au-coated PDG, consistently observed in all three membranes. The similar trend in the H₂/gas selectivity values continued upon deposition of 10 nm of Au while the average pore size reduced to 23.8 nm (Figure 2A,B). The permeance–molecular-weight relation fit equation became steeper,

$$P = 1.44 \times 10^7 \times m^{-0.61} \quad (3)$$

while the H₂/He selectivity did not change (Figure 3C). In order to elucidate the gas-transport mechanism, we performed

density-functional theory (DFT) calculations. When the pore size is large, the effect of gas–surface interactions on the transport properties of gas molecules, that is, permeance, through the pore is not significant. However, as the thickness of Au layer increases, the pores become narrower, and thus the interaction between the pore surface and the gas molecules increases, such that, below a certain threshold gas–surface interaction becomes the dominating factor in determining the gas permeance and selectivity. Increased gas–surface interactions explain the decrease in the H₂ permeance with increasing Au layer thickness (hence decreasing pore size) as shown in Figure 4A. As H₂ gas interacts more strongly with the Au surface due to decreasing pore size, it leads to a decreased permeance. The same rationale implies that gases interacting strongly with the surface are expected to have a lower permeance compared to the gases with weaker surface interactions. The increase in the H₂/gas selectivity with the decreasing pore size (Figures 3F–H) can be explained (Table S1, Supporting Information) by comparing the DFT predicted binding energies of gas molecules with the Au surface, that are −1.7, −5.3, −11.5, −17.7, and −21 kJ mol^{−1} for He, H₂, N₂, CH₄, and CO₂, respectively. N₂, CH₄, and CO₂ interact more strongly with the Au surface compared to H₂. As the pores become smaller with increasing membrane thickness, surface–gas interactions start to dominate, hence the permeance of N₂, CH₄, and CO₂ are expected to be smaller compared to the permeance of H₂, thus leading to higher H₂/gas selectivity with decreasing pore size. Accordingly, the slope of the permeance–molecular-weight curve becomes even larger at 20 nm of Au layer owing to the decreased pore size (Figure 3D):

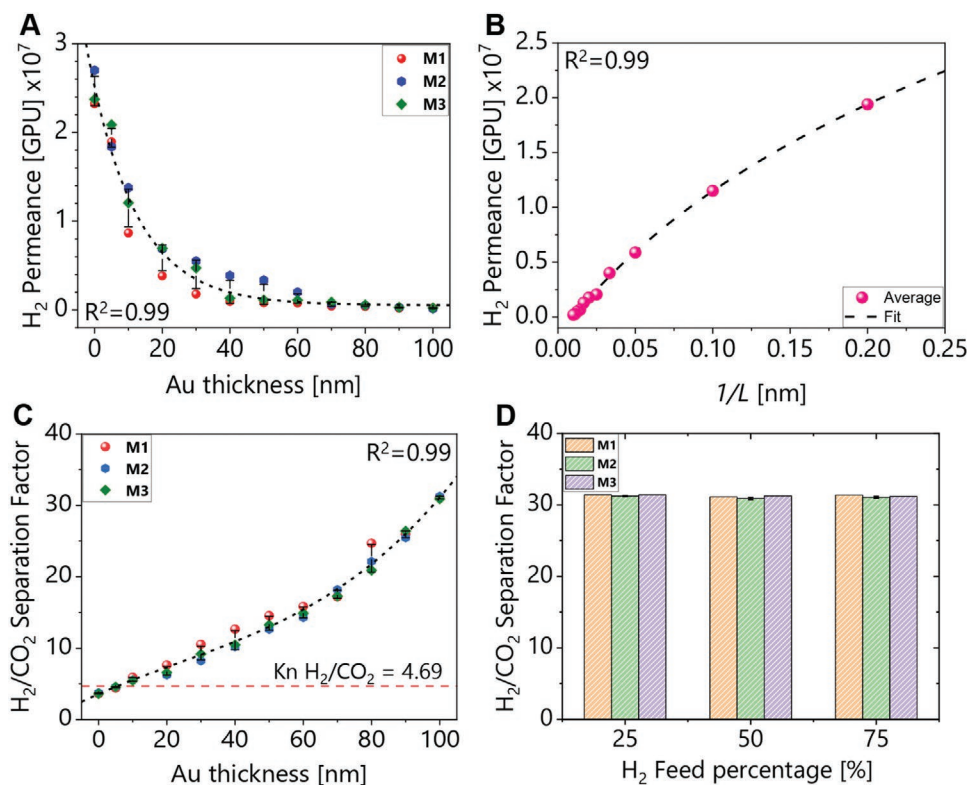


Figure 4. A) H₂ Permeance versus Au layer thickness for the membranes M1, M2, and M3. B) Average H₂ permeance versus 1/L; L is the thickness of the metal layer. C) H₂/CO₂ separation factor versus Au layer thickness for the membranes M1, M2, and M3. The dashed red line shows the Knudsen selectivity value for the H₂/CO₂ gas pair. D) H₂/CO₂ separation factors for the membranes M1, M2, and M3 at different feed gas ratios.

$$P = 7.48 \times 10^6 \times m^{-0.67} \quad (4)$$

On the other hand, H₂/He selectivity (Figure 3E) does not show a significant change with decreasing pore size, which can be attributed to the fact that the binding energies of these two gases are the lowest and much narrower pore sizes are needed for any surface effects to be observed in the H₂/He selectivity. The decrease in the permeance can be described by the blocking of the pores near the edges, as observed in the SEM images (Figure 2A) along with the increased thickness of the Au layer as well as the decreased pore size leading to stronger gas–surface interactions. In order to understand the relation between permeance and the Au layer thickness, we constructed a H₂ permeance versus Au layer thickness curve (Figure 4A). The H₂ permeance continues to decrease as more Au is deposited, which is expected since the flow changes from effusion to diffusion.^[25] However, the decrease in permeance becomes less evident as the thickness becomes larger than the mean free path of H₂ gas. The permeance versus thickness curve has an asymptotic relation,^[30,31]

$$P = 1.169 \times 10^8 / (1 + L) \quad (5)$$

where P is the permeance and the L is the thickness of the Au layer. As the value of L grows, P will continue to decrease eventually leading to an asymptote. This equation shows that permeance has negative relation with thickness. To understand the exact relationship between permeance versus Au thickness, we constructed H₂ permeance versus $1/L$ graph (Figure 4B). This relation fits the logarithmic relation^[30,31] of

$$P = 4.3204 \times 10^7 + 2.0291 \times 10^7 \times \ln\left(\frac{1}{L} + 0.1094\right) \quad (6)$$

indicating that at higher thickness (L) values, its effect on permeance (P) will be less as modeled before.^[30] We also measured the H₂/He and H₂/CO₂ separation factors to correlate with the calculated permselectivities (P_{H_2} / P_{gas}) (Figure 4C and Figure S3B, Supporting Information). In line with the calculated permselectivities, the H₂/He and H₂/CO₂ separation factors passed the Knudsen selectivity after 10 nm of Au deposition. The H₂/CO₂ separation factor increased almost linearly up to 70 nm of Au deposition. After this point, an abrupt increase in the slope is noted. The reason for the increase in slope is likely to be the transition in the gas-transport mechanism from surface diffusion to molecular sieving (Figure 1E) along with the enhanced gas–surface interactions. At 70 nm of Au layer, the pore size decreased below 5 nm, which is the starting point for molecular-sieving mechanism to happen (Figure 2D). A cubic relation between the H₂/CO₂ separation factor and thickness is obtained from the following fitting:^[7,31,32]

$$\alpha_{H_2/CO_2} = 3.575 + 0.2098L - 0.0015L^2 + 2.1648 \times 10^{-5} \times L^3 \quad (7)$$

where α_{H_2/CO_2} is the H₂/CO₂ separation factor and L is the Au layer thickness. The equation shows that the relation is more linear at low L values, however, at higher L values the quadratic and cubic portions of the curve start to have a higher effect. This fit curve almost perfectly coincides with the experimental

results of all three membranes. Eventually, at 100 nm of Au deposition, the TEM images revealed the average pore size of 3 nm, however, since the pore walls were found to be far from the ideal cylindrical shape due to the stepwise deposition, it is rather challenging to accurately calculate the pore size at this thickness (Figure S2, Supporting Information). We also note the formation of a large number of pores below 2 nm due to the stepwise deposition of gold layers leading to the molecular-sieving effect. By depositing 100 nm of Au, we were able to achieve an exceptional H₂/CO₂ separation factor of 31.3 at H₂ permeance of 2.23×10^5 GPU permeance (Table S2, Supporting Information), which is the highest value reported to date at this permeance range.^[14,28,33–44] Considering that more than 90% of H₂ is produced via steam reforming process, the H₂/CO₂ separation is also economically very important.^[45] Notably, this is the first demonstration of a large number of pores on the graphene surface with pore sizes below 3 nm for gas-separation applications. Moreover, the other two membranes showed very close results; the H₂/CO₂ separation factor of 31.1 and 30.9 at respective H₂ permeances of 2.13×10^5 and 1.47×10^5 GPU, proving reproducibility of our approach (Figure 4C). Furthermore, in order to verify that the H₂/CO₂ separation factor can be retained at different feed gas ratios, we compared the separation factors at H₂:CO₂ gas mixture ratios of 3:1, 1:1, and 1:3. All three membranes showed identical separation factors at different ratios of H₂ in the feed confirming the molecular-sieving-driven separation (Figure 4D). For the H₂/He separation, however, we did not observe a clear trend with the membrane thickness (Figure S3, Supporting Information). Once the H₂/He separation factors fall below the Knudsen value, it does not drop any further. This trend is expected as the H₂/He separation requires much smaller pores below 1 nm,^[46] thus further verifying the coexistence of surface diffusion and molecular-sieving mechanisms for the H₂/CO₂ separation.^[47] Compared to the recently reported Ni-coated PG membranes,^[29] M1, M2, and M3 not only show higher H₂/CO₂ selectivity in the same permeance range, but also the selectivity values are independent of the feed gas ratio.

Finally, we modeled the permeance–selectivity trade-off for the Au-coated graphene membranes (Figure 5). Our model equation fits the power relation^[5,6,48] of

$$P = 5923.9 \times \alpha^{-0.429} \quad (8)$$

where P is the permeance and α is the selectivity. The model shows how the performance of the Au-coated graphene membrane would evolve upon further deposition of Au and clearly demonstrates the impact of both pore size and thickness. It can be seen in Figure 5 that our model fit line intercepts with the inorganic tubular membranes such as silica, alumina, and zeolite membranes as our Au-coated membranes also have similar pore structure type and eventually they reach microporous tubular structure similar to silica type membranes. Thus, these results also confirm the validity of our fitted models. It should be noted that gold was chosen due to its inert nature, however, other cheaper metals such as aluminum, tungsten, nickel, chromium can also be used, where the gas–surface interactions would dictate the gas-transport properties. Furthermore, the desired permeance–selectivity can be obtained by simply tuning

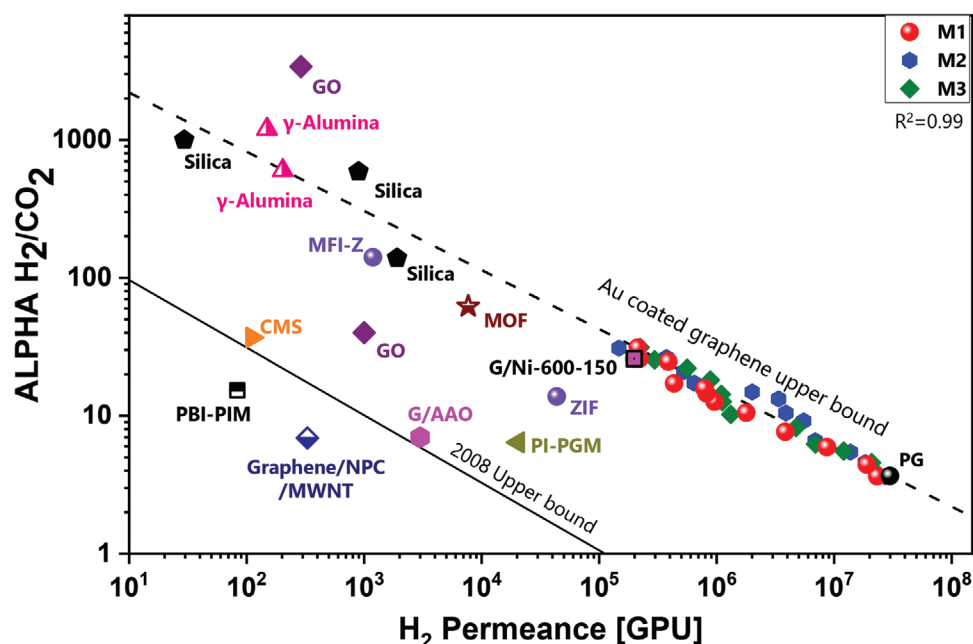


Figure 5. H_2/CO_2 separation performance of Au-coated double-layer graphene membranes compared to graphene oxide (GO),^[9,10] PG,^[8] polyimide–PG membrane (PI–PGM),^[28] carbon molecular-sieve membranes (CMS),^[34] polybenzimidazole–20% polymer of intrinsic microporosity (PBI–PIM),^[41] graphene/nanoporous carbon film/multiwalled carbon nanotubes (graphene/NPC/MWNT) membrane,^[14] graphene/nickel microislands (G/Ni-600-150),^[29] graphene on polished anodic aluminum oxide (G/AAO),^[26] metal–organic framework (MOF),^[40] zeolitic imidazole framework (ZIF),^[38] Mobil-5 zeolite (MFI-Z),^[35] silica,^[39,42,43] and γ alumina^[36,37] membranes. (Table S2, Supporting Information).

the thickness of the gold layer, which can be further decreased by starting with smaller pores on graphene.

3. Conclusions

We have shown that the creation of a large number of pores with pore sizes below 3 nm on the graphene surface could promote enhanced gas–surface interactions as well as the molecular-sieving effect. Moreover, the deposition of Au layer altered the graphene pore edge chemistry by enabling surface diffusion mechanism to achieve H_2 /gas selectivities above Knudsen selectivity despite having large pores (20–30 nm). In addition, through our systematic approach, we showed the possibility of achieving exceptional H_2/CO_2 selectivity values in the ultrahigh permeance range. Furthermore, we have successfully demonstrated that pore narrowing could be an alternative solution for increasing the gas selectivity in graphene membranes while retaining high permeance values. This strategy could guide the design of highly selective gas-separation membranes by using 2D materials as a high permeance support.

4. Experimental Section

Materials and Methods: A single-layer graphene on copper foil was purchased from Graphene EU and was used without any pretreatments. The holey silicon nitride (SiN_x) supports with 26 of 20×20 array 500–1000 nm pores were purchased by Norcada Inc., Canada. The SEM images were obtained by ThermoFischer Scios 2 SEM-FIB instrument using 5.0–20.0 kV accelerating voltage and 0.4 nA of current. The TEM images were obtained by FEI Tecnai Osiris instrument using 120–200 kV of accelerating voltage.

Graphene Transfer: Single-layer graphene on a copper foil was transferred using the previously reported facile photoresist-based method.^[29] Graphene on a copper foil was coated with Shipley S1800 photoresist (Microposit) using drop-casting, and allowed to dry overnight in an oven at 70 °C. Once the photoresist layer solidified, the copper film was etched using 0.5 M ammonium persulfate (Sigma-Aldrich) solution for 30 min. Then photoresist/graphene layer was washed several times by floating on deionized (DI) water before being transferred onto the holey SiN_x substrates. The SiN_x /graphene/photoresist was dried at room temperature for 1 h to completely remove the remaining water. Following the drying process, the SiN_x /graphene/photoresist was heated at 90 °C on a hot plate during 45–50 s. During the heating process, the photoresist layer melts and allowed for graphene to stick onto the substrate. Finally, the substrate with graphene was immersed into acetone solution and kept until the photoresist layer dissolved completely. Then the SiN_x /graphene was transferred into a fresh solution of acetone and kept for 30 min before being washed with ethanol. Double-layer graphene was transferred following the exact same procedure but without the heating step. Quality of the transferred graphene on SiN_x supports can be seen in the SEM images provided in Figure S1A,B, Supporting Information.

Supporting Information

Supporting Information is available from the Wiley Online Library or from the author.

Acknowledgements

The authors would like to acknowledge the EPFL Cmi Labs, Switzerland for access to the cleanroom. Authors acknowledge the support from the Swiss National Science Foundation (SNF) for funding this research (200021-175947). T.A. has performed all of the device fabrications and

membrane measurements. A.C. conceived and supervised the project, procured funds, and wrote the manuscript together with T.A.
Open access funding provided by Universite de Fribourg.

Conflict of Interest

The authors declare no conflict of interest.

Data Availability Statement

The data that support the findings of this study are openly available in Zenodo at <https://doi.org/10.5281/zenodo.5660751>.

Keywords

graphene membranes, H₂ permeation, H₂/CO₂ separation, pore tuning

Received: August 27, 2021

Revised: November 9, 2021

Published online: December 12, 2021

- [1] B. Freeman, *Angew. Chem., Int. Ed.* **2012**, *51*, 9485.
- [2] H. Strathmann, *An Introduction to Membrane Science and Technology*, Wiley-VCH, Weinheim, Germany **2011**.
- [3] D. M. Ruthven, *Gas Sep. Purif.* **1991**, *5*, 9.
- [4] A. B. Hincliffe, K. E. Porter, *Chem. Eng. Res. Des.* **2000**, *78*, 255.
- [5] L. M. Robeson, *J. Membr. Sci.* **1991**, *62*, 165.
- [6] L. M. Robeson, *J. Membr. Sci.* **2008**, *320*, 390.
- [7] H. B. Park, J. Kamcev, L. M. Robeson, M. Elimelech, B. D. Freeman, *Science* **2017**, *356*, eaab0530.
- [8] K. Celebi, J. Buchheim, R. M. Wyss, A. Droudian, P. Gasser, I. Shorubalko, J.-I. Kye, C. Lee, H. G. Park, *Science* **2014**, *344*, 289.
- [9] H. W. Kim, H. W. Yoon, S.-M. Yoon, B. M. Yoo, B. K. Ahn, Y. H. Cho, H. J. Shin, H. Yang, U. Paik, S. Kwon, J.-Y. Choi, H. B. Park, *Science* **2013**, *342*, 91.
- [10] H. Li, Z. Song, X. Zhang, Y. Huang, S. Li, Y. Mao, H. J. Ploehn, Y. Bao, M. Yu, *Science* **2013**, *342*, 95.
- [11] P. R. Kidambi, G. D. Nguyen, S. Zhang, Q. Chen, J. Kong, J. Warner, A.-P. Li, R. Karnik, *Adv. Mater.* **2018**, *30*, 1804977.
- [12] Q. Yang, Y. Su, C. Chi, C. T. Cherian, K. Huang, V. G. Kravets, F. C. Wang, J. C. Zhang, A. Pratt, A. N. Grigorenko, F. Guinea, A. K. Geim, R. R. Nair, *Nat. Mater.* **2017**, *16*, 1198.
- [13] Y. Yang, X. Yang, L. Liang, Y. Gao, H. Cheng, X. Li, M. Zou, R. Ma, Q. Yuan, X. Duan, *Science* **2019**, *364*, 1057.
- [14] W.-C. Lee, L. Bondaz, S. Huang, G. He, M. Dakhchoune, K. V. Agrawal, *J. Membr. Sci.* **2021**, *618*, 118745.
- [15] P. Bhol, S. Yadav, A. Altaee, M. Saxena, P. K. Misra, A. K. Samal, *ACS Appl. Nano Mater.* **2021**, *4*, 3274.
- [16] Y. Su, D. Liu, G. Yang, Q. Han, Y. Qian, Y. Liu, L. Wang, J. M. Razal, W. Lei, *ACS Appl. Mater. Interfaces* **2020**, *12*, 45453.
- [17] B. Sapkota, W. Liang, A. VahidMohammadi, R. Karnik, A. Noy, M. Wanunu, *Nat. Commun.* **2020**, *11*, 2747.
- [18] L. Ries, E. Petit, T. Michel, C. C. Diogo, C. Gervais, C. Salameh, M. Bechelany, S. Balme, P. Miele, N. Onofrio, D. Voiry, *Nat. Mater.* **2019**, *18*, 1112.
- [19] J. Kou, J. Yao, L. Wu, X. Zhou, H. Lu, F. Wu, J. Fan, *Phys. Chem. Chem. Phys.* **2016**, *18*, 22210.
- [20] E. H. Ang, J. W. Chew, *Chem. Mater.* **2019**, *31*, 10002.
- [21] D. Lere Keshebo, C.-P. Hu, C.-C. Hu, W.-S. Hung, C.-F. Wang, H.-C. Tsai, K.-R. Lee, J.-Y. Lai, *J. Membr. Sci.* **2021**, *634*, 119419.
- [22] P. Z. Sun, Q. Yang, W. J. Kuang, Y. V. Stebunov, W. Q. Xiong, J. Yu, R. R. Nair, M. I. Katsnelson, S. J. Yuan, I. V. Grigorieva, M. Lozada-Hidalgo, F. C. Wang, A. K. Geim, *Nature* **2020**, *579*, 229.
- [23] T. Yang, H. Lin, X. Zheng, K. P. Loh, B. Jia, *J. Mater. Chem. A* **2017**, *5*, 16537.
- [24] J. Buchheim, R. M. Wyss, I. Shorubalko, H. G. Park, *Nanoscale* **2016**, *8*, 8345.
- [25] E. A. Mason, B. Kronstadt, *J. Chem. Educ.* **1967**, *44*, 740.
- [26] M. S. H. Boutilier, D. Jang, J.-C. Idrobo, P. R. Kidambi, N. G. Hadjiconstantinou, R. Karnik, *ACS Nano* **2017**, *11*, 5726.
- [27] G. He, S. Huang, L. F. Villalobos, M. T. Vahdat, M. D. Guiver, J. Zhao, W.-C. Lee, M. Mensi, K. V. Agrawal, *Adv. Funct. Mater.* **2020**, *30*, 2003979.
- [28] K. Choi, A. Droudian, R. M. Wyss, K.-P. Schlichting, H. G. Park, *Sci. Adv.* **2018**, *4*, eaau0476.
- [29] T. Ashirov, A. Coskun, *Chem* **2021**, *7*, 2385.
- [30] G. Firpo, E. Angeli, P. Guida, R. L. Savio, L. Repetto, U. Valbusa, *Sci. Rep.* **2018**, *8*, 6345.
- [31] M. S. H. Boutilier, N. G. Hadjiconstantinou, R. Karnik, *Nanotechnology* **2017**, *28*, 184003.
- [32] J. Benito, J. Sánchez-Laínez, B. Zornoza, S. Martín, M. Carta, R. Malpass-Evans, C. Téllez, N. B. McKeown, J. Coronas, I. Gascón, *ChemSusChem* **2017**, *10*, 4014.
- [33] E. Lasseuguette, R. Malpass-Evans, M. Carta, N. B. McKeown, M.-C. Ferrari, *Membranes* **2018**, *8*, 132.
- [34] L. Lei, A. Lindbråthen, M. Hillestad, X. He, *J. Membr. Sci.* **2021**, *627*, 119241.
- [35] Z. Tang, J. Dong, T. M. Nenoff, *Langmuir* **2009**, *25*, 4848.
- [36] H. Lim, Y. Gu, S. T. Oyama, *J. Membr. Sci.* **2012**, *396*, 119.
- [37] S. Araki, N. Mohri, Y. Yoshimitsu, Y. Miyake, *J. Membr. Sci.* **2007**, *290*, 138.
- [38] Y. Qin, L. Xu, L. Liu, Z. Ding, *Ind. Eng. Chem. Res.* **2021**, *60*, 1387.
- [39] Y. Gu, P. Hacırlıoğlu, S. T. Oyama, *J. Membr. Sci.* **2008**, *310*, 28.
- [40] K. Yang, Y. Ban, A. Guo, M. Zhao, Y. Zhou, N. Cao, W. Yang, *J. Membr. Sci.* **2020**, *611*, 118419.
- [41] J. Sánchez-Laínez, B. Zornoza, M. Carta, R. Malpass-Evans, N. B. McKeown, C. Téllez, J. Coronas, *Ind. Eng. Chem. Res.* **2018**, *57*, 16909.
- [42] R. M. de Vos, H. Verweij, *J. Membr. Sci.* **1998**, *143*, 37.
- [43] S. Battersby, T. Tasaki, S. Smart, B. Ladewig, S. Liu, M. C. Duke, V. Rudolph, J. C. Diniz da Costa, *J. Membr. Sci.* **2009**, *329*, 91.
- [44] K. Shimizu, T. Ohba, *Phys. Chem. Chem. Phys.* **2017**, *19*, 18201.
- [45] B. Zornoza, C. Casado, A. Navajas, in *Renewable Hydrogen Technologies* (Eds: L. M. Gandía, G. Arzamendi, P. M. Diéguez), Elsevier, Amsterdam, The Netherlands **2013**, p. 245.
- [46] P. Rezaee, H. R. Naeij, *Carbon* **2020**, *157*, 779.
- [47] Z. Yuan, R. P. Misra, A. G. Rajan, M. S. Strano, D. Blankschtein, *ACS Nano* **2019**, *13*, 11809.
- [48] M. U. Siddiqui, A. F. M. Arif, S. Bashmal, *Membranes* **2016**, *6*, 40.